REVEALING HIDDEN DRAWINGS IN LEONARDO'S 'THE VIRGIN OF THE ROCKS' FROM MACRO X-RAY FLUORESCENCE SCANNING DATA THROUGH ELEMENT LINE LOCALISATION

Su Yan[⋆], *Jun-Jie Huang*[⋆], *Nathan Daly*[†], *Catherine Higgitt*[†], *Pier Luigi Dragotti*[⋆]

[⋆] Department of Electrical and Electronic Engineering, Imperial College London
[†] Scientific Department, The National Gallery

ABSTRACT

Macro X-Ray Fluorescence (XRF) scanning is an increasingly widely used imaging technique for the non-invasive detection and mapping of chemical elements in Old Master paintings. Existing approaches for XRF signal analysis require varying degrees of expert user input. They are mainly based on peak fitting at fixed energies associated with each element and require the target elements to be selected manually. In this paper, we propose a new method that can process macro XRF scanning data from paintings fully automatically. The method consists of two parts: 1) detecting pulses in an XRF spectrum using Finite Rate of Innovation (FRI) theory; 2) producing the distribution maps for each element automatically identified in the painting. The results presented show the ability of our method to detect weak or partially overlapping signals and more excitingly to have visualisation of underdrawing in a masterpiece by Leonardo da Vinci.

Index Terms— Signal processing, Macro X-ray Fluorescence scanning, Finite Rate of Innovation, Old Master Paintings

1. INTRODUCTION

Easel painting is one of the most influential and important forms of art around the world. A painting is created by applying pigments (in a binder) onto a support such as a canvas or wooden panel, building up the final image layer by layer. Therefore, in the final painting there may be invisible layers concealed beneath subsequent paint applications. Hidden features can include an artist's preliminary sketches (or underdrawing), rough laying-in of the composition, earlier version of the design that were modified in the final version or even another painting. Visualising these features is of great interest to artists, scientists and the public but is an extremely challenging task as these details are concealed by subsequent layers of paint that cannot be disturbed or removed.

Macro X-Ray Fluorescence (XRF) scanning is one of the imaging techniques that can be used non-invasively to reveal the invisible sub-surface details in paintings [1]. A macro XRF scanning device sequentially illuminates sub-millimetre spots (or pixels) of a painting with a primary X-ray beam that can penetrate through surface layers, exciting the emission of X-ray photons with energies that are specific to the elements present within the pigments used in the painting. Theoretically, each element actually emits a series of characteristic element lines relating to electronic transition processes in the atoms and the number of X-ray emission lines increase with atomic number. Due to the effect of the XRF device, each element line is broadened into a narrow pulse [2]. The X-ray photons emitted at each pixel are detected as a spectrum consisting of a collection of pulses due to all of the elements in this region (see Fig. 1 for an example, where the x-axis is energy in electron volts (eV) and the y-axis is the number of photons counted per second). Hence, the presence of an element can be confirmed in a particular region if all the expected element line pulses corresponding to that element are detected within the XRF spectrum, which is called XRF spectrum deconvolution. However, paintings are created by complex pigment mixtures and therefore many elements are present at each single pixel. As a consequence of that it is quite common that pulses related to elements of interest in a painting overlap.

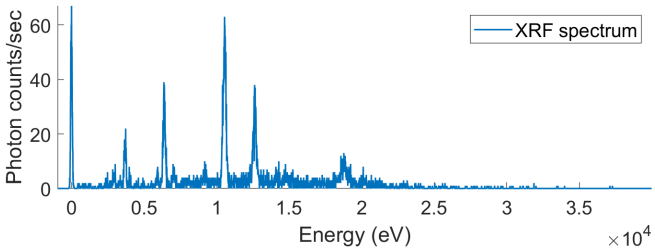

Fig. 1: XRF spectrum by averaging a 3-by-3 array of pixels (pixel size is 350 um) in a painting.

Many approaches have been proposed for XRF spectrum analysis and deconvolution. P. Van Espen *et al.* [3] created AXIL; V.A. Solé *et al.* [4] developed 'PyMca' in Python; M. Alfeld and K. Janssens [5] developed 'Datamuncher' in IDL; D.M. Conover [6] proposed a method using non-linear regression; Bruker Corporation also provides deconvolution and quantification tools in the software for their commercial macro XRF scanning instrument. The basic idea of these approaches is to use linear or non-linear regression to fit the XRF spectrum with pulse shape functions (Gaussian functions) [7]. The fitting requires knowledge of the number, variances (widths) and means (locations) of the Gaussian functions. The variances can be obtained by measurements [6] or existing models [3, 5]. The number and means of the Gaussian functions can be determined if the existing elements in the XRF spectrum are known. Existing approaches all require users to input the target elements into the software before analysing the XRF spectrum. But the problem is that the selection of elements by the user has great effects on the accuracy of the results. In this paper, a new fully automatic method based on Finite Rate of Innovation (FRI) theory [8, 9] is proposed to process XRF spectra. It automatically detects the pulses within XRF spectra and produces the element distribution maps for the painting.

This work is in part supported by EPSRC grant EP/R032785/1. Su Yan is supported by China Scholarship Council (CSC) scholarship.

2. PROPERTIES OF XRF SPECTRA

The collected XRF spectra contain information about the elemental composition of the scanned painting in the form of a sequence of pulses with different amplitudes, widths and positions. Fig. 1 shows an example of an XRF spectrum obtained by averaging a 3-by-3 array of pixels (pixel size is 350 µm) from a scan of a painting. Four properties of XRF spectra and their associated challenges should be exploited to enable a robust algorithm to identify element lines:

1. Due to the effect of the device, each element line is widened and can be well modelled by a Gaussian pulse centred at the right energy level [2]. It can therefore be difficult to deconvolute element lines close in energy due to pulse overlap, especially when one element line is of relatively low intensity compared to the neighbouring lines.
2. The pulse shape of the element lines is a function of photon energy and the element lines broaden with energy [2, 6]. This imposes an extra difficulty in detecting the element lines. Given a reference pulse at energy E_{ref} in electron volts (eV) with full width at half maximum (FWHM) FWHM_{ref}, the pulse width of an element line at energy E can be expressed as [10]:
$$\text{FWHM}_E = \left(2.5(E - E_{\text{ref}}) + \text{FWHM}_{\text{ref}}^2\right)^{1/2} . \quad (1)$$
3. The relative intensities of the characteristic lines for different elements may change depending on where the atoms of interest are within the layer structures of the scanned painting due to secondary effects [11]. For example, lower energy photons emitted by the atoms of an element during ionisation are more likely than higher energy photons to be absorbed or scattered before reaching the detector. This suggests that, unlike their energies, the relative intensities of the characteristic lines for a given element are variable and therefore not reliable for element identification.
4. In macro XRF scanning, the detected XRF spectra can be noisy as shown in Fig. 1. This is because paintings are scanned pixel by pixel and the number of photons collected by the detector is proportional to parameters like beam size, pixel size, and dwell time per pixel. Trying to achieve an XRF spectrum with good signal-to-noise-ratio (SNR) for each sub-millimetre pixel makes scanning an entire painting very time-consuming. Moreover, the signal from elements deep in the painting are partially attenuated by elements in the layers above and therefore produce only a small number of photons.

3. PROPOSED METHOD

In this paper, we propose to first detect all potential pulses from the XRF spectra with FRI and matrix pencil methods. The detected pulses will then be used to determine the presence of specific elements in the painting.

3.1. FRI Based Pulse Detection

The width of an unknown pulse can be well modelled by Eq. (1) with a given pulse as reference. In this paper, the first pulse in XRF spectrum is used as the reference pulse because it is known to be at the location of zero energy level and does not belong to any element.

Since the XRF spectrum of a single pixel contains $L = 4096$ values and the pulse width changes with energy, the XRF spectrum cannot be properly processed as a whole. Instead we operate on blocks of $l = 300$ values each and use a sliding window with overlap $l/2$. Our pulse detection algorithm is then applied to each window. Moreover, we assume that the pulse shape remains the same in each window region. Thus, the spectrum in each window can be represented as a linear combination of several pulses with the same shape and a noise term:

Algorithm 1: Pulse detection algorithm

```
Input: XRF spectrum of one pixel
Output:
for each sliding window do
    for K ← K_max to K_min do
        Calculate the coefficients {c_{m,n}}.
        Calculate the moments {s_m}.
        Retrieve {t_k} with matrix pencil method [12].
        Retrieve θ = {{a_k}, σ} or θ = {a_k} with least
          squares.
        if ∀θ ≥ 0 then
            Keep the detection results.
            Break the loop.
Apply the noise threshold to all detected pulses.
```

$$y_n = \sum_{k=1}^{K} a_k \varphi[n - t_k] + \epsilon[n] , \quad (2)$$

where y_n is the XRF spectrum with $n = 0, 1, ..., l-1$; K is the number of pulses; $\varphi[n]$ is the pulse shape; a_k and t_k are the amplitudes and locations of the pulses; $\epsilon[n]$ is the noise. Then, the XRF spectrum in each window can be regarded as a signal with finite rate of innovation (FRI) [8].

We approximate each $\varphi[n]$ with exponential splines (E-splines) and therefore, together with their shifted versions they can approximately reproduce exponentials:

$$\sum_{n\in\mathbb{Z}} c_{m,n}\varphi(n - t) \approx e^{\alpha_m t} , \quad (3)$$

where $m = 0, 1, ..., P$; $\alpha_m = \alpha_0 + m\lambda$; and $\alpha_0, \lambda \in \mathbb{C}$. The coefficients $\{c_{m,n}\}$ can be calculated using [13]

$$c_{m,n} = e^{\alpha_m n} \frac{e^{\alpha_m t}}{\sum_{n\in\mathbb{Z}} e^{\alpha_m n}\varphi(n - t)} . \quad (4)$$

Then a linear combination of y_n with the coefficients $c_{m,n}$ is calculated as

$$s_m = \sum_n c_{m,n} y_n . \quad (5)$$

And using Eq. (3) and Eq. (2), we obtain:

$$s_m = \sum_n c_{m,n} y_n \approx \sum_k \alpha_k e^{\alpha_m t_k} = \sum_{k=1}^{K} b_k u_k^m , \quad (6)$$

where $b_k = a_k e^{\alpha_0 t_k}$ and $u_k = e^{\lambda t_k}$. Therefore, pulse amplitudes $\{a_k\}_{k=1}^K$ and locations $\{t_k\}_{k=1}^K$ can be retrieved from the moments s_m by matrix pencil method [9, 12].

Matrix pencil [12] requires the number of pulses K to be known, while our goal is to detect and localise an unknown number of potential pulses within a sliding window. Leveraging the fact that matrix pencil is very fast, we propose to solve this model selection problem

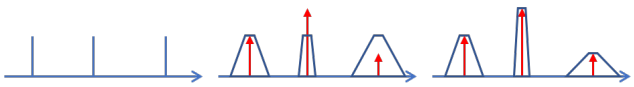

(a) Vector $\boldsymbol{x}_M$ (b) Vector $\hat{\boldsymbol{y}}$ (c) Vector $\hat{\boldsymbol{z}}$

Fig. 2: Vectors for EC and EQ, where red spikes are the detected pulses.

by examining the number of pulses from a maximum number K_{max} to a minimum number K_{min}. With a given K, matrix pencil method retrieves pulse locations $\{t_k\}$. Pulse amplitudes $\{a_k\}$ can be obtained by the least squares fitting given the observed XRF spectrum, detected pulse locations $\{t_k\}$ and the pulse shape. A constant term σ can be optionally added to the least squares fitting to model the background noise. Since all the pulse amplitudes and the noise term should not be negative, the optimal pulse number K is selected with the condition that $\{a_k\}$ and σ are all non-negative. Our algorithm detects the pulses with fitting the background noise firstly. With K decreasing from K_{max} to K_{min}, the optimal K, $\{a_k\}$ and σ will be obtained when the condition is met. If not, the algorithm will switch to the detection without fitting noise. The optimal K and a_k will still be chosen when the condition is met. Note that, the detection algorithm should be repeated on every window region of the XRF spectrum. Finally, a noise threshold is applied and those detected pulses with amplitudes lower than the threshold will be removed. Our pulse detection algorithm has been summarised in Algorithm 1.

3.2. Element Distribution Maps

After retrieving pulses with locations $\{t_k\}$ and amplitudes $\{a_k\}$ from the XRF spectra, they are used to determine the distributions of elements present in the painting. Two parameters are introduced here, which are element confidence (EC) and element quantity (EQ). EC shows the confidence that an element exists in a certain region and EQ indicates the relative quantity of that element. Both the EC and EQ are calculated based on the pulse detection results and this is done pixel by pixel. The EC map and EQ map of one element can be created if the EC and EQ of that element are calculated for all the pixels in the painting.

Three vectors are created for computing the EC and EQ of element M. These are element line (EL) vector $\boldsymbol{x}_M$, detected location (DL) vector $\boldsymbol{y}$ and detected pulse (DP) vector $\boldsymbol{z}$. Vector $\boldsymbol{x}_M$ has a value of one at the locations of the characteristic lines of element M:

$$x_{M,i} = \begin{cases} 1, \ i = \text{characteristic lines of element M}, \\ 0, \ \text{otherwise}. \end{cases} \tag{7}$$

An example of $\boldsymbol{x}_M$ is plotted in Fig. 2a. Vector $\boldsymbol{y}$ has a value of one at the locations of the detected pulses:

$$y_i = \begin{cases} 1, \ i = t_k, \\ 0, \ \text{otherwise}, \end{cases} \tag{8}$$

and vector $\boldsymbol{z}$ has the values of the corresponding detected amplitudes at detected pulses locations:

$$z_i = \begin{cases} a_k, \ i = t_k, \\ 0, \ \text{otherwise}. \end{cases} \tag{9}$$

In addition, each spike (non-zero value) in $\boldsymbol{y}$ and $\boldsymbol{z}$ is given a shape, represented by the shape vector $\boldsymbol{s}_k$ with width d_k, to model

Fig. 3: Leonardo da Vinci, 'The Virgin of the Rocks' [14]. Highlighted is the region of an XRF dataset collected on the painting with an M6 Bruker JETSTREAM instrument (30 W Rh anode at 50 kV and 600 µA, 60 mm^2 Si drift detector, and data collected with 350 µm beam and pixel size and 10 ms dwell time).

the uncertainty of the pulse detection algorithm. The width d_k is chosen to be odd numbers and determined by the pulse amplitude a_k. A detected pulse with lower amplitude will be given a shape s_k with larger d_k because detecting a weaker pulse is more likely to have errors. The shape vector $\boldsymbol{s}_k$ is then created as:

$$\boldsymbol{s}_k = [\frac{1}{h}, \frac{2}{h}, \cdots, \frac{h}{h}, 1, \frac{h}{h}, \cdots, \frac{2}{h}, \frac{1}{h}], \tag{10}$$

where $h = (d_k - 1)/2$. The spikes in $\boldsymbol{y}$ and $\boldsymbol{z}$ are then broaden using the corresponding shape vectors. The resulting vectors are denoted as $\hat{\boldsymbol{y}}$ and $\hat{\boldsymbol{z}}$ respectively. An example can be found in Fig. 2.

Element Confidence: The EC of element M is defined as the normalised inner product between $\boldsymbol{x}_M$ and $\hat{\boldsymbol{y}}$:

$$EC = \frac{\langle \boldsymbol{x}_M, \hat{\boldsymbol{y}} \rangle}{\|\boldsymbol{x}_M\| \|\hat{\boldsymbol{y}}\|}, \tag{11}$$

Those elements not present in the pixel will have $EC = 0$ and those elements having all the characteristic lines detected at the right energies will achieve an EC close to 1.

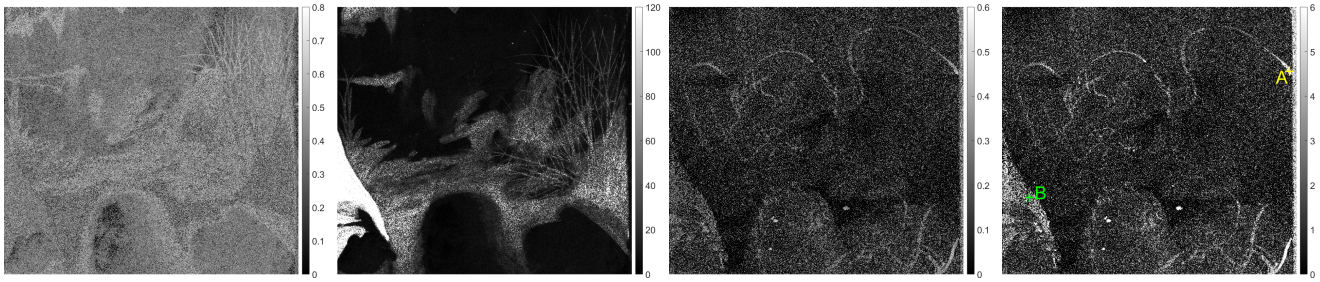

(a) Cu EC map (b) Cu EQ map (c) Zn EC map (d) Zn EQ map

Fig. 4: Element maps of copper (Cu) and zinc (Zn), pixel A is on the angel wing and pixel B is on the drapery.

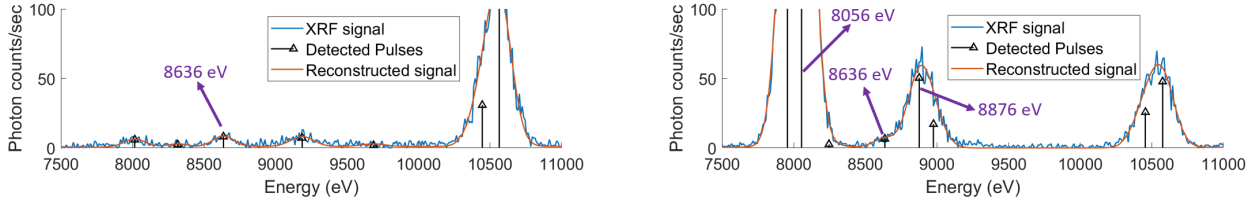

(a) Pulse detection result of Pixel A on the angel wing

(b) Pulse detection result of Pixel B on the drapery

Fig. 5: The pulse detection results of two pixels on the draperies.

Element Quantity: The EQ of element M is defined as the inner product of vector $\boldsymbol{x}_M$ and $\hat{\boldsymbol{z}}$:

$$EQ = \langle \boldsymbol{x}_M, \hat{\boldsymbol{z}} \rangle \,, \tag{12}$$

which is the weighted summation of the amplitudes of the detected pulses corresponding to element M.

4. RESULTS

A region of Leonardo da Vinci's painting 'The Virgin of the Rocks' [14], highlighted in Fig. 3 was scanned with Bruker M6 macro XRF scanning equipment at the National Gallery. Our proposed algorithm was applied on the collected XRF spectra and used to generate element distribution maps for further analysis.

Fig. 4 illustrates the element maps of copper (Cu) and zinc (Zn) produced by our algorithm. The Cu EC map shown in Fig. 4a has values around 0.5 at most of the pixels, suggesting that copper is present throughout this particular region of the painting. The Cu EQ map in Fig. 4b shows clear bright regions, relating to the Virgin's drapery and the foliage in the painting. This indicates that the intensities of Cu at the pixels of the areas of foliage and especially for the pixels of the draperies on the left border of the painting are much higher than in the other pixels. In previous examination, it was found that the foliage includes the copper-based mineral azurite [15]. The element maps of Zn in Fig. 4c and Fig. 4d show more unexpected results. Some pixels with values about 0.3 in the Zn EC map create what appear to be lines. Those lines are even more clear in the Zn EQ map. These Zn-containing shapes do not correspond to any features visible in the final painting composition. Instead, they are related to underdrawing of planned figures (the wings and the head of an angel are clearly visible) that was then painted over. Although previous technical examination of the painting had revealed the existence of underdrawing for an unrealised figure of the Virgin, the planned figures of the angel and Christ child were unknown prior to undertaking the macro XRF scanning [15, 16]. It is also of interest to note that photon counts for the lines of the underdrawing are very small and yet our method has been able to find the pulses related to the Zn element, which was confirmed in a micro-sample of paint mounted in cross-section using scanning electron microscopy with energy-dispersive X-ray analysis (SEM-EDX). The Zn EQ map also indicates that the azurite used in the underlayer for the drapery contains a little Zn which, although not confirmed in a micro-sample, is a common impurity in azurite mineral sources.

To demonstrate the ability of our method to deconvolute two nearby pulses, we now focus on pixels 'A' on the angel wing and 'B' on the drapery shown in Fig. 4d. Cu has two major element lines at energies about 8037 and 8905 eV and Zn has one major element line at energy about 8627 eV [17]. The pulse detection results of the pixels A and B in the range of $[7500, 11000]$ eV are shown in Fig. 5 and resolution of the XRF spectrum is 10 eV. For pixel A, one pulse detected in 8635 eV belongs to Zn. For pixel B, two detected pulses in 8056 eV and 8876 eV correspond to Cu and one pulse in 8636 eV belongs to Zn. It is shown that although the XRF spectrum is noisy and the Zn pulse is weak and covered by a much stronger Cu pulse, our proposed algorithm is still able to detect both of them correctly and the resulting maps accurately show the distribution and amount of Cu and Zn in the area examined.

5. CONCLUSION

In this paper, we proposed an automatic approach for XRF spectrum deconvolution which was applied to visualise underdrawing in an Old Master painting. Our two-stage approach first detects all the potential pulses in an XRF spectrum using variations of FRI and matrix pencil methods. Given the detected pulses in each pixel, element distribution maps including EC maps and EQ maps were produced for an entire scanned region of a painting. The resulting maps obtained on 'The Virgin of the Rocks' by Leonardo da Vinci show that our proposed method can address the challenge of both very noisy data and convoluted signals common in macro XRF scanning in the cultural heritage community, especially when features of interest are hidden in deep layers.

6. REFERENCES

[1] P. Ricciardi, S. Legrand, G. Bertolotti, and K. Janssens, "Macro X-ray fluorescence (MA-XRF) scanning of illuminated manuscript fragments: potentialities and challenges," *Microchemical Journal*, vol. 124, pp. 785–791, 2016.

[2] J.I. Goldstein, D.E. Newbury, J.R. Michael, N.W. Ritchie, J.He.J. Scott, and D.C. Joy, *Scanning electron microscopy and X-ray microanalysis*, Springer, 2017.

[3] P. Van Espen, H. Nullens, and F. Adams, "A computer analysis of x-ray fluorescence spectra," *Nuclear Instruments and Methods*, vol. 142, no. 1-2, pp. 243–250, 1977.

[4] V.A. Solé, E. Papillon, M. Cotte, P. Walter, and J. Susini, "A multiplatform code for the analysis of energy-dispersive x-ray fluorescence spectra," *Spectrochimica Acta Part B: Atomic Spectroscopy*, vol. 62, no. 1, pp. 63–68, 2007.

[5] M. Alfeld and K. Janssens, "Strategies for processing megapixel x-ray fluorescence hyperspectral data: a case study on a version of caravaggio's painting supper at emmaus," *Journal of analytical atomic spectrometry*, vol. 30, no. 3, pp. 777–789, 2015.

[6] D.M. Conover, *Fusion of Reflectance and X-ray Fluorescence Imaging Spectroscopy Data for the Improved Identification of Artists' Materials*, Ph.D. thesis, The George Washington University, 2015.

[7] R. Van Grieken and A. Markowicz, *Handbook of X-ray Spectrometry*, CRC press, 2001.

[8] M. Vetterli, P. Marziliano, and T. Blu, "Sampling signals with finite rate of innovation," *IEEE transactions on Signal Processing*, vol. 50, no. 6, pp. 1417–1428, 2002.

[9] J.A. Urigüen, T. Blu, and P.L. Dragotti, "FRI sampling with arbitrary kernels," *IEEE Transactions on Signal Processing*, vol. 61, no. 21, pp. 5310–5323, 2013.

[10] C.E. Fiori and D.E. Newbury, "Artifacts observed in energy dispersive x-ray spectrometry in the scanning electron microscope," *Scanning Electron Microscopy*, vol. 1, no. 1978, pp. 401, 1978.

[11] B. Beckhoff, B. Kanngießer, N. Langhoff, R. Wedell, and H. Wolff, *Handbook of practical X-ray fluorescence analysis*, Springer Science & Business Media, 2007.

[12] Y. Hua and T.K. Sarkar, "Matrix pencil method for estimating parameters of exponentially damped/undamped sinusoids in noise," *IEEE Transactions on Acoustics, Speech, and Signal Processing*, vol. 38, no. 5, pp. 814–824, 1990.

[13] J. Oñativia Bravo, *Sampling and reconstruction of finite rate of innovations signals with applications in neuroscience and sparse representation*, Ph.D. thesis, Imperial College London, 2015.

[14] Leonardo da Vinci, "The Virgin of the Rocks (NG1093)," about 1491/2-9 and 1506-8, oil on poplar, 189.5 x 120 cm, The National Gallery, London.

[15] L. Keith, A. Roy, R. Morrison, and P. Schade, "Leonardo da Vinci's "Virgin of the Rocks": Treatment, Technique and Display," *National Gallery Technical Bulletin*, vol. 32, pp. 32–56, 2011.

[16] The National Gallery, "Unlocking Leonardo," `https://www.nationalgallery.org.uk/exhibitions/leonardo-experience-a-masterpiece/unlocking-leonardo`.

[17] J.A. Bearden, "X-ray wavelengths," *Reviews of Modern Physics*, vol. 39, no. 1, pp. 78, 1967.